# Construction of 6G Omni-Scenario Knowledge Base for On-Demand Service Using Channel Knowledge Map

**Zifan Sha[1], Changle Li[1,†], Wenwei Yue[1], Xiaojian Yang[1], Yuchuan Fu[1], Luqiao Wang[1], Nan Cheng[1], Mahdi Boloursaz Mashhadi[2], Zhili Sun[2]**

[1]State Key Laboratory of Integrated Services Networks, Xidian University
[2]5GIC & 6GIC, Institute for Communication Systems (ICS), University of Surrey
{zfsha, yxj, 23011110200}@stu.xidian.edu.cn,
{clli}@mail.xidian.edu.cn,
{wwyue, ycfu, nancheng}@xidian.edu.cn,
{m.boloursazmashhadi, z.sun}@surrey.ac.uk

## Abstract

With the rapid evolution of 6G networks, the need for on-demand service across diverse scenarios continues to grow. However, a key challenge lies in the lack of a structured knowledge infrastructure that can possess the capability for standardized representation and accurately reflect the comprehensive 6G scenarios. To address this, we propose OSOD 6G, a 6G omni-scenario knowledge base empowered by Channel Knowledge Map (CKM), designed to capture and infer the essential features of wireless channels under varying environments. Firstly, by elucidating the intrinsic relationships among subject, environment, requirement, and knowledge through an ontological framework, OSOD 6G covers seven representative scenarios including multi-stage urban areas, plain, mountain, and ocean. Secondly, we deploy heterogeneous transmitters such as omnidirectional base stations, directional base stations, and satellites across distinct urban development stages, and densely position receivers both in aerial and terrestrial domains. Then, CKM inference is used to extract channel data, which is then filtered, structured, and indexed under a unified schema. The resulting dataset includes 759,590 structured entries, enabling efficient scenario-aware inference. Finally, simulation results reveal significant channel characteristic variations across different deployment configurations and environmental types, underscoring the necessity for service customization. Moreover, in handling large-scale CKM data, the XGBoost model demonstrates superior fitting accuracy compared with the baseline, achieving an R-squared of 94.94% and a root mean square error (RMSE) of 0.8394.

## Introduction

As 6G technology advances toward practical deployment by 2030, its ambitions extend beyond achieving ultra-high data rates and low latency. A central objective is to develop intelligent network architectures that can adapt dynamically to complex and heterogeneous scenarios while enabling on-demand service regulation (Wang et al. 2023). In this context, the seamless integration of space, air, ground, and sea has become a critical research focus in the 6G era (Xiao et al. 2024). However, current approaches, including channel modeling, data-driven analysis, and localized knowledge-based optimization, remain isolated in scope and fall short of addressing the comprehensive and adaptive requirements of next-generation networks (Serghiou et al. 2022). These constraints are reflected in the following aspects:

- **Lack of unified representation and standardized description across 6G omni-scenario:** Existing studies often focus on isolated environments such as urban microcells (Das et al. 2024) or satellite communications (Bakhsh et al. 2024), without offering a unified framework capable of adapting to diverse conditions. The abstraction of interrelationships among physical environments, communication entities, and service requirements remains insufficient, limiting the applicability of existing approaches in realizing the converged, holistic vision of 6G.
- **Inefficiency in acquiring large-scale and dynamic channel data across diverse scenarios:** As 6G networks extend to cover environments spanning air, space, ground, and sea, the communication characteristics become increasingly dynamic and complex. Existing methods mainly rely on physical measurements or localized simulations (Cano et al. 2021), which are constrained by cost, time, and equipment availability. These constraints hinder the development of scalable and diverse channel datasets.
- **Absence of inference mechanisms for channel knowledge:** Current approaches remain focused on data analysis, without systematically incorporating the concept of "knowledge" or its inferencing capabilities (Chaccour et al. 2025). This limitation impedes end-to-end service processes, including transformation from data to knowledge, and finally decision-making.

Specifically, the contributions are made as follows:

- We propose **an ontology-based framework for the 6G omni-scenario knowledge base (OSOD 6G)**, covering a wide range of physical environments including urban, plain, mountainous, and oceanic contexts. The ontological structure reveals deep interrelationships among subject, environment, requirement, and knowledge, providing a solid foundation for effective knowledge inference

and precise matching of service demands with available resources.

- We develop **a CKM-enabled methodology for building OSOD 6G**, where multi-scenario channel data are generated through ray-tracing simulations. By leveraging the Channel Knowledge Map (CKM), this method enables comprehensive inference and visualization of channel characteristics, facilitating the construction of a structured, scalable knowledge base tailored for 6G networks.
- We conduct **simulations to validate the knowledge inference capabilities of OSOD 6G across diverse scenarios**, including various urban types and receiver altitudes. Moreover, the CKM fitting performance is rigorously evaluated, demonstrating high accuracy and robustness in modeling complex channel dynamics under different environmental and deployment conditions.

The remainder of this paper is organized as follows. Section  introduces the ontology-based framework for OSOD 6G. Section  presents the construction of OSOD 6G based on the CKM theory. Section  provides visualization and simulation-based validation of OSOD 6G, focusing on multi-dimensional inference across diverse omni-scenario settings. Finally, Section  concludes the paper and outlines directions for future research.

## Ontology-based framework for OSOD 6G

OSOD 6G is an academic knowledge base designed for 6G omni-scenario. In this section, we elucidate the ontological structure and data schema of OSOD 6G, followed by a statistical analysis of its derived static datasets. Notably, while the OSOD 6G knowledge base is inherently dynamic and extensible, the extraction of static datasets serves the purpose of data-driven model training and analysis, facilitating the integration and validation of on-demand service capabilities across 6G scenarios.

### Ontology structure of OSOD 6G

The ontology structure of OSOD 6G is illustrated graphically in Figure 1 to provide an intuitive representation. At its core, the central node OSOD 6G comprises four primary entity classes: Subject, Environment, Requirement, and Knowledge.

- **Subject** includes two key attributes: Type of Subject (covering transmitters, receivers, and transceivers) and Location of Subject, which is defined by three spatial dimensions: lateral, longitudinal, and vertical.
- **Environment** consists of Geographic Environment (plain, mountain, ocean), Altitude Space (ground-based or air-based), and Urban Type (suburban, urban, dense urban, and urban high-rise).
- **Requirement** captures both Resource Type (including base stations, aerial base stations, and satellites) and Requirement Indicators (such as channel capacity, communication bandwidth, latency, and access count).

Table 1: Statistics of OSOD 6G dataset across diverse scenarios.

| Environment | Type of urban | Base station | Aerial base station | Satellite | No. of samples |
|---|---|---|---|---|---|
| Plain | Suburban | ✓ | ✓ | ✓ | 58,267 |
| | Urban | ✓ | ✓ | ✓ | 48,543 |
| | Dense urban | ✓ | ✓ | ✓ | 150,093 |
| | Urban high rise | ✓ | ✓ | ✓ | 130,725 |
| | Other areas | ✓ | × | ✓ | 215,512 |
| Mountain | - | × | ✓ | ✓ | 30,237 |
| Ocean | - | × | × | ✓ | 126,213 |
| Omni-scenario (Sum up) | All areas | ✓ | ✓ | ✓ | 759,590 |

- **Knowledge** incorporates various channel parameters, including channel capacity, received power, noise power, signal-to-noise ratio, time of arrival, and path loss.

Furthermore, six types of relationships are defined to establish interconnections among these entities: consists of, has property, exists in, is combined with, reflects, and deduces to.

### Statistics of OSOD 6G dataset

As previously described, the OSOD 6G dataset encompasses three representative geographical environments: plain, mountainous, and oceanic regions. Within the plain environment, four urban typologies are considered, i.e., suburban, urban, dense urban, and urban high-rise.

The OSOD 6G dataset encompasses entities and statistical samples across a wide range of scenarios, as summarized in Table 1. It includes 120, 000 user receiving terminals deployed across three altitude layers, i.e., 2 m, 150 m, and 300 m.

In total, the constructed dataset contains approximately 500, 000 samples. To support validation in specific subscenarios, we have additionally curated a subset comprising 10, 663 samples, which has been made publicly available[1]. This subset represents a simplified setting with a single base station deployed at a single altitude layer, enabling focused performance evaluation and comparative analysis.

## Construction of OSOD 6G Enabled by Channel Knowledge Map

Building upon the ontology framework, this section utilizes the CKM to construct OSOD 6G. Specifically, we detail the development of urban environment models, the design of

[1]https://github.com/shazifan/OSOD-6G_A-6G-Omni-Scenario-Knowledge-Base-for-On-Demand-Service.git.

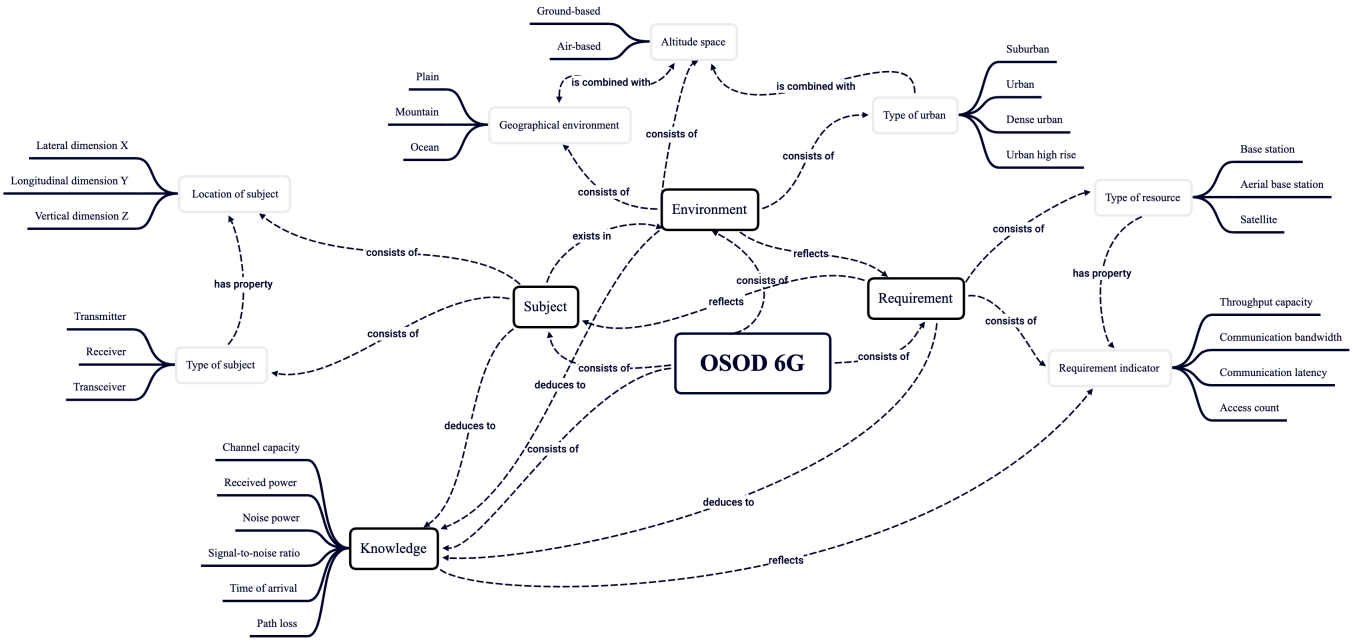


Figure 1: The ontology structure of OSOD 6G.

channel modeling processes, and the fitting of the CKM. Finally, the effectiveness of the resulting knowledge base is illustrated through comprehensive CKM visualizations.

## Urban model

Urban areas are constructed based on the standardized urban model defined in ITU-R Recommendation P.1410, as issued by the International Telecommunication Union (ITU) (ITU-R-P.1410-2 2003). The model parameters:

- The ratio of built-up land area to total land area, denoted as $\alpha \in [0.1, 0.8]$;
- The average building density, expressed as the number of buildings per square kilometer, $\beta \in [100, 750]$;
- Building heights, which follow a Rayleigh distribution with standard deviation $\gamma$.

## Channel modeling

We employ the Ray-Tracing algorithm (Wang et al. 2025) to compute the channel model. This method constructs signal propagation paths in a three-dimensional environment and calculates the variations in physical parameters resulting from interactions between the signal paths and surrounding surfaces. In a MIMO system with $M$ transmit antennas and $N$ receive antennas, the channel impulse response between the $i$-th transmit antenna and the $j$-th receive antenna is expressed in Eq. (1), while the corresponding frequency response of the system is provided in Eq. (2).

$$g_{n,m}(t) = \sum_{l=1}^{L} \sqrt{P_{R,l}} e^{i\theta_l} \delta\left(t - \tau_l\right) \ , \tag{1}$$

$$h_{n,m} = \sum_{l=1}^{L} \sqrt{P_{R,l}} e^{i\theta t} \cdot e^{-2\pi i f_0 \tau_l} \ , \tag{2}$$

$$H = \begin{bmatrix} h_{1,1} & h_{1,2} & \cdots & h_{1,M} \\ h_{2,1} & h_{2,2} & \cdots & h_{2,M} \\ \vdots & \vdots & \ddots & \vdots \\ h_{N,1} & h_{N,2} & \cdots & h_{N,M} \end{bmatrix}, \tag{3}$$

$$C = \log_2 \left[ \det \left( I + \frac{\rho}{M} H H^T \right) \right], \tag{4}$$

where $L$ denotes the number of ray paths received at the receiver, and $\delta$ represents the unit impulse function. For the $l$-th ray path, $P(R, l)$, $\theta_l$, and $\tau_l$ denote the received power, phase angle, and the relative delay with respect to the direct path, respectively. $\rho$ is the receiver's signal-to-noise ratio (SNR), $H$ is the $N \times M$ channel matrix, $H^T$ denotes its conjugate transpose, and $I$ is the $M \times M$ identity matrix. The channel capacity $C$ is regarded as a key knowledge output within then CKM.

## CKM model fitting

The construction of the CKM fundamentally constitutes an interpolation or extrapolation task within the spatial domain. Current approaches typically do not explicitly exploit the inherent correlation between environmental geometric structures and the measured channel data (Zeng et al. 2024). However, in localized regions, it is feasible to approximate the channel characteristics in a target location by leveraging data from spatially adjacent areas. Within the channel dataset $\mathbb{D}$, as defined in Eq. (5), a channel subset $D\left(X_\delta, Y_\delta, Z_\delta\right) \in \mathbb{D}$ can be extracted, as detailed in Eq. (6). $N_{bs}$ denotes the total number of aerial base stations, and $N_{bs}$ represents the total number of receiving terminals. The coordinates of the $\zeta$-th base station are given by $(X_\zeta, Y_\zeta, Z_\zeta)$, while the coordinate of the $\varepsilon$-th receiver associated with that base station is $(x_{\zeta,\varepsilon}, y_{\zeta,\varepsilon}, z_{\zeta,\varepsilon})$. For each

transmitter–receiver pair, the corresponding channel capacity is denoted as $C_{\zeta,\varepsilon}$, and the average time of arrival is represented as $\bar{t}_{\zeta,\varepsilon}$. Through $N_{bs}$ simulation iterations, it becomes possible to generate a comprehensive dataset characterizing the urban MIMO channel, incorporating both aerial and terrestrial base stations deployed at varying spatial locations.

$$\mathbb{D} = \{D \mid D\left(X_\zeta, Y_\zeta, Z_\zeta\right), \zeta \in [1, N_{bs}]\}, \tag{5}$$

$$\begin{aligned} D\left(X_\zeta, Y_\zeta, Z_\zeta\right) = \{&(x_{\zeta,\varepsilon}, y_{\zeta,\varepsilon}, z_{\zeta,\varepsilon}, env_{\zeta,\varepsilon}, C_{\zeta,\varepsilon}, P_{R\zeta,\varepsilon}, \\ &\rho_{\zeta,\varepsilon}, \bar{t}_{\zeta,\varepsilon}, band_{\zeta,\varepsilon}, delay_{\zeta,\varepsilon}), \\ &\varepsilon \in [1, N_{re}],\}, \end{aligned} \tag{6}$$

The receiver positions associated with the $\zeta$-th base station in the dataset $D\left(X_\delta, Y_\delta, Z_\delta\right)$ are used as input features to train the model. The corresponding outputs for each receiver include the channel capacity $C_{\zeta,\varepsilon}$, average received power $P_{R\zeta,\varepsilon}$, signal-to-noise ratio $\rho_{\zeta,\varepsilon}$, average arrival time $\bar{t}_{\zeta,\varepsilon}$, bandwidth $band_{\zeta,\varepsilon}$, and delay $delay_{\zeta,\varepsilon}$. The training process is formalized in Eq. (7):

$$(C, P_R, \rho, \bar{t}, band, delay, \bar{t}) = \mathrm{CKM}\left((x_\zeta, y_\zeta, z_\zeta)\right), \tag{7}$$

XGBoost (eXtreme Gradient Boosting) is a machine learning algorithm built upon the gradient boosting decision tree framework (Li et al. 2022). It is renowned for its robustness in handling diverse data types and for its high efficiency in training and prediction on large-scale datasets. The objective function of XGBoost is defined in Eq(8):

$$obj = \sum_{i=1}^{n} Loss\left(y_i, \widehat{y}_i\right) + \sum_{k=1}^{K} \Omega\left(f_k\right), \tag{8}$$

where $n$ represents the total number of samples, $K$ denotes the number of trees, $Loss\left(y_i, \widehat{y}_i\right)$ is the loss function measuring the difference between the true and predicted values, and $\Omega(f_k)$ is the regularization term that penalizes the complexity of the model to prevent overfitting.

## Verification and visualization of OSOD 6G

### Omni-scenario visualization and verification

First, we visualized the omni-scenario encompassing space-air-ground-sea domains, accounting for diverse terrains and urban typologies. We utilize Wireless InSite (Remcom 2022) to model a comprehensive physical environment and to visualize channel capacity across diverse omni-scenario settings. The visualization is illustrated in Figure 2.

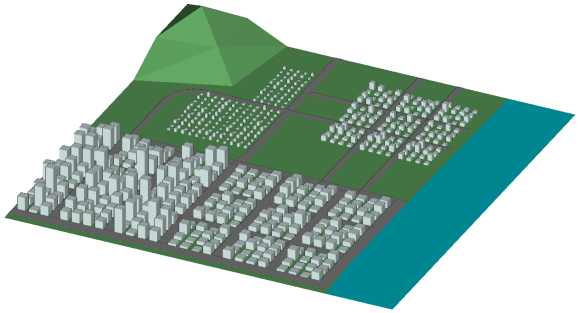

Figure 2: Omni-scenario visualization.

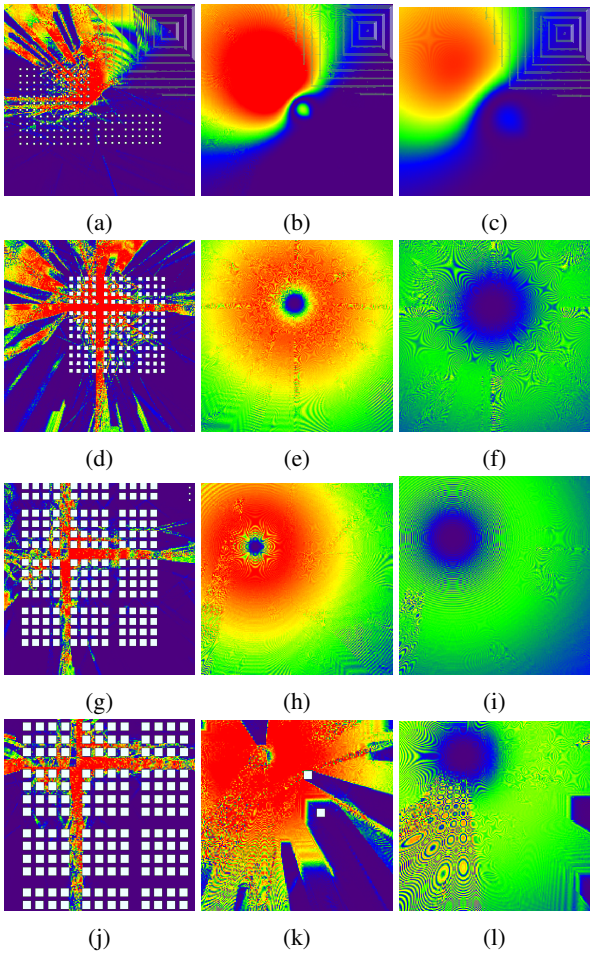


Figure 3: Visualization of the CKM across different urban typologies and altitudes from the terrestrial base station: a) Suburban-2m; b) Suburban-150m; c) Suburban-300m; d) Urban-2m; e) Urban-150m; f) Urban-300m; g) Dense urban-2m; h) Dense urban-150m; i) Dense urban-300m; j) Urban high rise-2m; k) Urban high rise-150m; l) Urban high rise-300m.

### CKM inference verification

Subsequently, we employ ray tracing to infer the channel capacity of the scenario, thereby constructing the CKM.

**When the signal transmitter is a terrestrial base station**, the visualization results of the CKM across different urban typologies and altitudes are shown in Figure 3. Specifically, Figures 3a, 3b, and 3c show the CKMs in the Suburban area at 2 m, 150 m, and 300 m, respectively. Figures 3d, 3e, and 3f correspond to the Urban area at 2 m, 150 m, and 300 m. Figures 3g, 3h, and 3i depict the CKMs in the Dense urban area at 2 m, 150 m, and 300 m. Figures 3j, 3k, and 3l illustrate the CKMs in the Urban high rise area at 2 m, 150 m, and 300 m, respectively.

**When the transmitter is an aerial base station**, the corresponding knowledge map visualization is presented in Figure 4. Specifically, Figures 4a, 4b, and 4c show the CKMs in the Suburban area at 2 m, 150 m, and 300 m, respectively. Figures 4d, 4e, and 4f correspond to the Urban area at 2 m, 150 m, and 300 m. Figures 4g, 4h, and 4i depict the CKMs in the Dense urban area at 2 m, 150 m, and 300 m. Figures 4j, 4k, and 4l illustrate the CKMs in the Urban high rise area at 2 m, 150 m, and 300 m, respectively.

## CKM fitting performance verification

**From a quantitative perspective, we further validated the fitting performance of XGBoost**.

Table 2–5 present the mean and variance of CKM fitting results for different urban scenarios, altitude levels, and signal transmitters, respectively.

**From the mean capacity standpoint**, the four urban environments, serving as deployment hubs for all signal sources, exhibit higher mean channel capacity compared to mountainous, oceanic, and other plain regions. Among the latter three, mountainous area benefits from its altitude advantage, allowing for superior reception of satellite and aerial base station signals, thereby achieving the highest mean channel capacity. In contrast, oceanic region, which rely solely on satellite connectivity, exhibits the lowest mean channel capacity.

**Regarding variance**, among the four urban types, suburban areas demonstrate the highest channel capacity variance due to the dual-directional antennas deployed at suburban base stations, which significantly reduce signal stability. In contrast, mountainous regions, benefiting from their superior satellite signal reception, exhibit the lowest channel capacity variance.

In Figure 5, Deep Neural Network (DNN) (Zhang et al. 2016), Fully Convolutional Networks (FCN) (Shelhamer, Long, and Darrell 2016) and Convolutional Neural Network (CNN) (Li et al. 2021) have long training time and low accuracy, and Support Vector Machine (SVM) (Noble 2006) has short training time and high accuracy. XGBoost's determination coefficient R-squared can reach 94.94% and Root Mean Square error (RMSE) is 0.8394. SVM training speed and accuracy are also excellent, but it is difficult to deal with large-scale datasets. It is sensitive to missing data and difficult to adjust SVM parameters. Through meticulous hyperparameter tuning, XGBoost can better accommodate diverse data characteristics, demonstrating rapid and accurate channel capacity prediction in the construction of CKM.

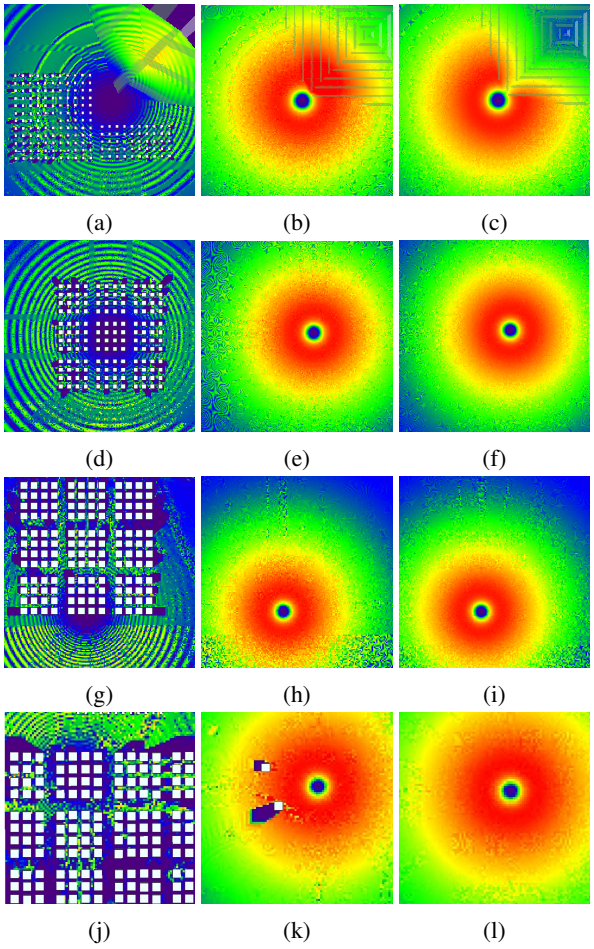


Figure 4: Visualization of the CKM across different urban typologies and altitudes from the aerial base station: a) Suburban-2m; b) Suburban-150m; c) Suburban-300m; d) Urban-2m; e) Urban-150m; f) Urban-300m; g) Dense urban-2m; h) Dense urban-150m; i) Dense urban-300m; j) Urban high rise-2m; k) Urban high rise-150m; l) Urban high rise-300m.

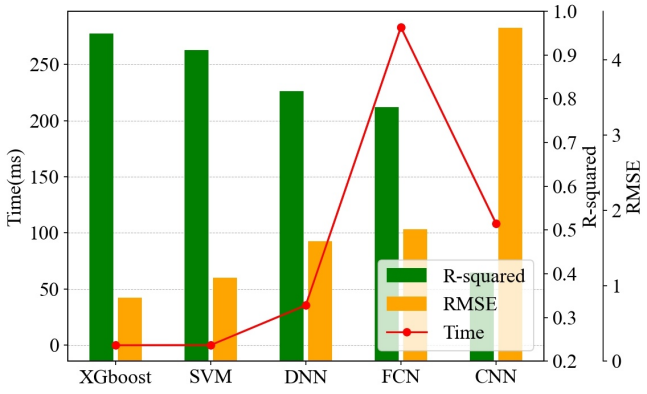


Figure 5: Performance comparison under various regression prediction models.

Table 2: Mean and variance of CKM fitting results for suburban.

| | **BS** | | **ABS** | | **Satellite** | |
|---|---|---|---|---|---|---|
| Suburban | Mean (Mbit/s) | Var $(\text{Mbit/s})^2$ | Mean (Mbit/s) | Var $(\text{Mbit/s})^2$ | Mean (Mbit/s) | Var $(\text{Mbit/s})^2$ |
| Layer 1-(2m) | 378.096 | 163247.16 | 219.361 | 12093.795 | 431.299 | 18904.766 |
| Layer 2-(150m) | 233.837 | 38115.854 | 418.645 | 27615.825 | 473.357 | 16813.169 |
| Layer 3-(300m) | 118.164 | 13121.769 | 388.084 | 21639.517 | 457.228 | 18681.611 |

Table 3: Mean and variance of CKM fitting results for urban.

| | **BS** | | **ABS** | | **Satellite** | |
|---|---|---|---|---|---|---|
| Urban | Mean (Mbit/s) | Var $(\text{Mbit/s})^2$ | Mean (Mbit/s) | Var $(\text{Mbit/s})^2$ | Mean (Mbit/s) | Var $(\text{Mbit/s})^2$ |
| Layer 1-(2m) | 433.727 | 123360.07 | 199.578 | 9957.588 | 353.165 | 8600.854 |
| Layer 2-(150m) | 537.280 | 14837.642 | 379.390 | 24615.320 | 395.966 | 1054.266 |
| Layer 3-(300m) | 298.349 | 1846.1396 | 377.921 | 23788.860 | 392.82 | 6372.495 |

Table 4: Mean and variance of CKM fitting results for dense urban.

| | **BS** | | **ABS** | | **Satellite** | |
|---|---|---|---|---|---|---|
| Dense urban | Mean (Mbit/s) | Var $(\text{Mbit/s})^2$ | Mean (Mbit/s) | Var $(\text{Mbit/s})^2$ | Mean (Mbit/s) | Var $(\text{Mbit/s})^2$ |
| Layer 1-(2m) | 215.513 | 101046.31 | 192.812 | 12996.962 | 323.628 | 16442.523 |
| Layer 2-(150m) | 505.603 | 24543.487 | 439.282 | 26035.857 | 396.930 | 985.520 |
| Layer 3-(300m) | 296.297 | 2047.463 | 438.240 | 25521.935 | 378.320 | 1274.020 |

Table 5: Mean and variance of CKM fitting results for urban high rise.

| | **BS** | | **ABS** | | **Satellite** | |
|---|---|---|---|---|---|---|
| Urban high rise | Mean (Mbit/s) | Var $(\text{Mbit/s})^2$ | Mean (Mbit/s) | Var $(\text{Mbit/s})^2$ | Mean (Mbit/s) | Var $(\text{Mbit/s})^2$ |
| Layer 1-(2m) | 183.259 | 79967.689 | 151.785 | 12411.569 | 309.125 | 20350.754 |
| Layer 2-(150m) | 501.798 | 77432.833 | 433.920 | 31791.429 | 397.291 | 1495.338 |
| Layer 3-(300m) | 316.494 | 14343.546 | 434.010 | 31102.256 | 395.54 | 5795.441 |

## Conclusions

This paper presents OSOD 6G, a CKM-enabled omni-scenario knowledge base supporting on-demand service in 6G networks. Firstly, a structured ontology is developed to formalize the relationships among subjects, environments, requirements, and knowledge, enabling standardized and extensible representation. Secondly, leveraging CKM-driven inference, OSOD 6G facilitates accurate knowledge extraction and intuitive visualization. Afterwards, the simulation results reveal substantial variations in channel characteristics across different deployment configurations and environmental types, highlighting the critical need for on-demand service. Meanwhile, the XGBoost model improves CKM fitting performance, achieving an R-squared value of 94.94% and a root mean square error (RMSE) of 0.8394. Future work will refine knowledge-driven inference for integration of communication, sensing, computing, and control in 6G on-demand service.

## Acknowledgments

This work was supported by the National Natural Science Foundation of China (62231020), the Innovation Capability Support Program of Shaanxi (2024RS-CXTD-01), and the Technology Innovation Leading Program of Shaanxi (2023KXJ-116).

## References

Bakhsh, Z. M.; Omid, Y.; Chen, G.; Kayhan, F.; Ma, Y.; and Tafazolli, R. 2024. Multi-Satellite MIMO Systems for Direct Satellite-to-Device Communications: A Survey. *IEEE Communications Surveys & Tutorials*, 1–1.

Cano, C.; Sim, G. H.; Asadi, A.; and Vilajosana, X. 2021. A Channel Measurement Campaign for mmWave Communication in Industrial Settings. *IEEE Transactions on Wireless Communications*, 20(1): 299–315.

Chaccour, C.; Saad, W.; Debbah, M.; Han, Z.; and Vincent Poor, H. 2025. Less Data, More Knowledge: Building Next-Generation Semantic Communication Networks. *IEEE Communications Surveys & Tutorials*, 27(1): 37–76.

Das, S.; Sen, D.; Viterbo, E.; Majumdar, C.; Chavva, A. K. R.; Sharma, D.; and Nigam, A. 2024. Ambit-Process Based Channel Model for Urban Microcellular Communication at 140 GHz. *IEEE Transactions on Wireless Communications*, 23(5): 3959–3974.

ITU-R-P.1410-2. 2003. Propagation data and prediction methods for the design of terrestrial broadband millimetric radio access systems.

Li, W. T.; Tang, H. S.; Cui, C.; Hei, Y. Q.; and Shi, X. W. 2022. Efficient Online Data-Driven Enhanced-XGBoost Method for Antenna Optimization. *IEEE Transactions on Antennas and Propagation*, 70(7): 4953–4964.

Li, Z.; Liu, F.; Yang, W.; Peng, S.; and Zhou, J. 2021. A survey of convolutional neural networks: analysis, applications, and prospects. *IEEE transactions on neural networks and learning systems*, 33(12): 6999–7019.

Noble, W. S. 2006. What is a support vector machine? *Nature biotechnology*, 24(12): 1565–1567.

Remcom. 2022. Wireless EM Propagation Software-Wireless InSite.

Serghiou, D.; Khalily, M.; Brown, T. W. C.; and Tafazolli, R. 2022. Terahertz Channel Propagation Phenomena, Measurement Techniques and Modeling for 6G Wireless Communication Applications: A Survey, Open Challenges and Future Research Directions. *IEEE Communications Surveys & Tutorials*, 24(4): 1957–1996.

Shelhamer, E.; Long, J.; and Darrell, T. 2016. Fully convolutional networks for semantic segmentation. *IEEE transactions on pattern analysis and machine intelligence*, 39(4): 640–651.

Wang, C.-X.; You, X.; Gao, X.; Zhu, X.; Li, Z.; Zhang, C.; Wang, H.; Huang, Y.; Chen, Y.; Haas, H.; Thompson, J. S.; Larsson, E. G.; Renzo, M. D.; Tong, W.; Zhu, P.; Shen, X.; Poor, H. V.; and Hanzo, L. 2023. On the Road to 6G: Visions, Requirements, Key Technologies, and Testbeds. *IEEE Communications Surveys & Tutorials*, 25(2): 905–974.

Wang, S.; Gao, S.; Yang, W.; Zhang, Q.; Loh, T. H.; Yang, Y.; and Qin, F. 2025. A Physics-Informed Deep Ray Tracing Network for Regional Channel Impulse Response Estimation. *IEEE Transactions on Wireless Communications*, 1–1.

Xiao, Y.; Ye, Z.; Wu, M.; Li, H.; Xiao, M.; Alouini, M.-S.; Al-Hourani, A.; and Cioni, S. 2024. Space-Air-Ground Integrated Wireless Networks for 6G: Basics, Key Technologies, and Future Trends. *IEEE Journal on Selected Areas in Communications*, 42(12): 3327–3354.

Zeng, Y.; Chen, J.; Xu, J.; Wu, D.; Xu, X.; Jin, S.; Gao, X.; Gesbert, D.; Cui, S.; and Zhang, R. 2024. A Tutorial on Environment-Aware Communications via Channel Knowledge Map for 6G. *IEEE Communications Surveys & Tutorials*, 26(3): 1478–1519.

Zhang, J.; Zheng, Y.; Qi, D.; Li, R.; and Yi, X. 2016. DNN-based prediction model for spatio-temporal data. In *Proceedings of the 24th ACM SIGSPATIAL international conference on advances in geographic information systems*, 1–4.